Intrinsic flexoelectricity of van der Waals epitaxial thin films

Longlong Shu,[1] Zhiguo Wang,[1] Renhong Liang,[1] Zhen Zhang,[1] Shengwen Shu,[2] Changxin Tang,[3] Fei Li,[4] Ren-Kui Zheng,[1] Shanming Ke,[1,*] and Gustau Catalan[5,6,†]

[1]*School of Materials Science and Engineering, Nanchang University, Nanchang, People's Republic of China*

[2]*College of Electrical Engineering and Automation, Fuzhou University, Fuzhou 350108, China*

[3]*Institute of Photovoltaics, Nanchang University, Nanchang, People's Republic of China*

[4]*Electronic Materials Research Laboratory, Key Laboratory of the Ministry of Education and International Center for Dielectric Research, Xi'an Jiao Tong University, Xi'an, People's Republic of China*

[5]*Institucio Catalana de Recerca i Estudis Avançats (ICREA), Barcelona, Catalonia*

[6]*Institut Catala de Nanociencia i Nanotecnologia (ICN2), Consejo Superior de Investigaciones Científicas and The Barcelona Institute of Science and Technology (CSIC–BIST), Campus Universitat Autonoma de Barcelona, Barcelona, Catalonia*

(Received 8 February 2022; revised 30 June 2022; accepted 11 July 2022; published 20 July 2022)

The direct measurement of flexoelectric coefficients in epitaxial thin films is an unresolved problem, due to the clamping effect of substrates which induces a net strain (and hence parasitic piezoelectricity) in addition to strain gradients and flexoelectricity. Herein, we propose and demonstrate the use of van der Waals epitaxy as a successful strategy for measuring the intrinsic (clamping-free = flexoelectric coefficients of epitaxial thin films. We have made, measured, and compared $BaTiO_3$ and $SrTiO_3$ thin film capacitor heterostructures grown both by conventional oxide-on-oxide epitaxy and by van der Waals oxide-on-mica epitaxy, and found that, whereas the former is dominated by parasitic piezoelectricity, the response of the latter is truly flexoelectric. The results are backed by theoretical calculations of the film-substrate mechanical interaction, as well as by direct measurements that confirm the strain-free state of the films. van der Waals epitaxy thus emerges as powerful new tool in the study of flexoelectricity and, in particular, they finally allow exploring flexoelectric phenomena at the nanoscale (where strain gradients are highest) with direct experimental knowledge of the actual flexoelectric coefficients of thin films.

DOI: 10.1103/PhysRevB.106.024108

I. INTRODUCTION

Flexoelectricity refers to the generation of electric polarization when a material is subjected to strain gradient (in contrast to piezoelectricity, which is generated by uniform strain) [1–9]. Any material with bound charges or interface charges can, in principle, be flexoelectric, irrespective of their crystalline structures [10–12]. Flexoelectricity is not exclusive of solid dielectrics [13–15], but a rather universal property, having been observed or predicted in liquid crystals [16–18], biological materials [19–21], semiconductors [22–24], and even metals [25]. In terms of physics, strain gradient has a distinctive scaling effect, being inversely proportional to materials' size, which results in nanoscale flexoelectricity being of utmost significance [26–28]. The strain gradient of thin films can readily approach the order of $10^7\ m^{-1}$ upon lattice mismatch between epitaxial films and their substrate, or under indentation by the tip of a scanning-probe microscope [29–31]. In addition, flexoelectricity can couple to other physical properties and bring out emerging behaviors, such as flexoresistance [32], flexophotovoltaic effect [33], photoflexoelectric effect [22], fracture asymmetry [34], flexomagnetism [35], etc.

Despite its growing relevance, our direct experimental knowledge of flexoelectricity in thin films is limited. In particular, the basic problem of measuring the flexoelectric coefficients of thin film materials has not yet been resolved. In bulk, direct measurement of flexoelectricity normally involves bending a material and measuring its bending-induced surface charge density, but in thin films it is difficult to perform such measurements because thin films are normally attached to rigid substrates with strong chemical bonds [36,37]. In order to bend the film, it is therefore necessary to also bend its substrate. Such bending not only generates strain gradient (curvature) but also strain on the surface (compressive on the concave side, tensile on the convex side) thus also to the film attached to it. Due to this strain, piezoelectricity can also be generated, even when the thin film in question is nominally nonpiezoelectric [38,39]. The only estimates of flexoelectricity in thin films are indirect, and rely on the flexoelectric switching of ferroelectric films using the tip of an atomic force microscope [30]. Besides being indirect and quantitatively imprecise (the strain gradient generated by the tip pressure is never measured but numerically estimated [40]), such measurements are only suitable for ultrathin ferroelectric films with out-of-plane polarization, which are a tiny subset.

*Corresponding author: ksm@ncu.edu.cn

†Corresponding author: gustau.catalan@icn2.cat

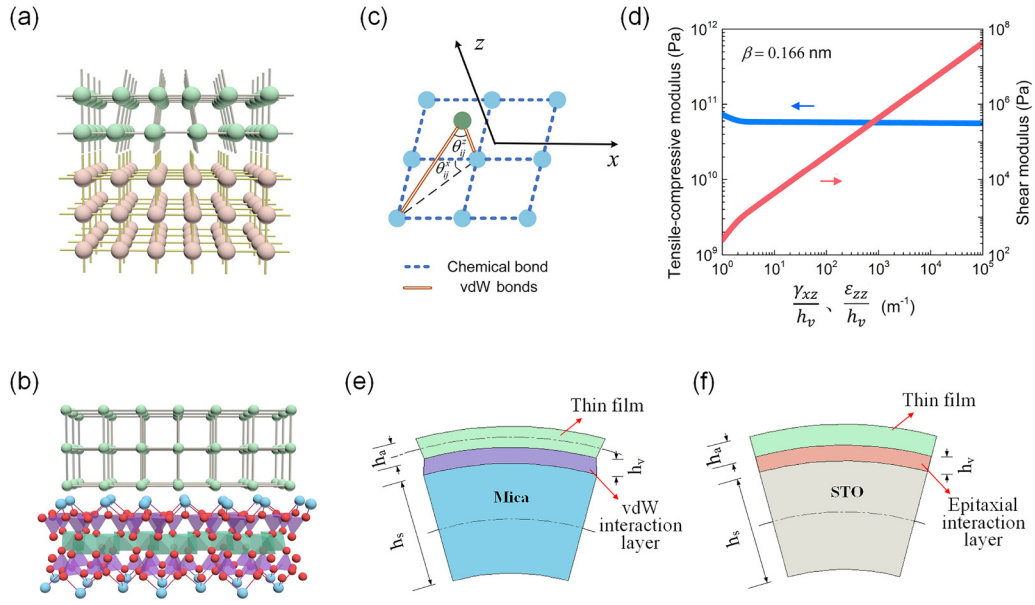

FIG. 1. Schematic illustration of (a) conventional and (b) van der Waals epitaxy. (c) Definition of angle θ_{ij}^{x} and θ_{ij}^{z}. (d) The relationship between the tensile-compressive, shear modulus, and strain gradient for vdW layer. Deformation characteristics of (e) mica substrate, BTO thin films, and (f) STO substrate, BTO thin films after bending.

Alternatively, the influence of the substrate may be eliminated by using free-standing thin films [41]. However, clamping such thin films on one side while applying a mechanical load on the other in order to bend them is experimentally impractical: free-standing films are just too flimsy. In an ideal world, one would therefore want to combine the handling practicality of substrate-backed films with the unstrained response of free-standing films. Herein, we report a general approach to achieve such a goal by exploiting van der Waals epitaxy, whereby films are grown on flexible mica substrates, bonded with only weak van der Waals (vdW) interactions between the thin film and the substrate. Our theoretical calculations indicate that the weak bonding in mica-based vdW thin films can effectively remove the substrate clamping effect so that, upon bending the substrate, the film glides over the surface without stretching or compressing. This ensures that the film experiences bending but no net strain, allowing the flexoelectric coefficients of the films to be accurately measured using the same standard experiment setups used for bulk materials [27]. We confirm this theoretical prediction by performing and comparing measurements of archetypal oxide thin films ($SrTiO_3$ and $BaTiO_3$) grown by conventional and van der Waals epitaxy.

In conventional thin film epitaxy, strong chemical bonding is formed between film and substrate [Fig. 1(a)] [42,43]. In addition, the epitaxial strain induced by lattice mismatch between film and substrate can lead to a change of the ground state, interdiffusion, or accumulation of defects at interfaces. As a result, epitaxial films rarely exhibit bulklike properties. van der Waals (vdW) epitaxy [44–50] provides a route to mitigate these problems. In vdW epitaxy, the epilayer has the single-crystal-like crystalline coherence of standard epitaxial films, yet the interface is only weakly bonded by vdW interactions. The typical vdW bonding energy (40–70 meV) is much smaller than covalent (200–6000 meV) or ionic bonding energies (7000–40 000 meV), resulting in a longer interfacial bonding distance without intermixing [Fig. 1(b)], and a reduced ability of the substrate to stress the film [51]. Our expectation is therefore that a vdW-bonded film should glide over the surface of the substrate as it is bent.

II. PHYSICAL MODEL AND FINITE ELEMENT METHOD SIMULATIONS

We start by building the theory of vdW interaction with respect to bending deformation. In a simple atomic model, the upper and lower atomic layers are assumed to be connected by vdW interactions [Fig. 1(b)]. At time t_0, the two layers connected by vdW force maintain a stable state with minimum energy, and at time t_1, a relative displacement occurs. The equivalent shear modulus is determined by the sliding of the upper atomic layer relative to the bottom layer in the in-plane direction, while the equivalent tensile-compressive modulus could be determined by the out-of-plane direction of motion.

The potential energy between two atoms in two adjacent layers is given by the Lennard-Jones potential function as follows [52]:

$$U_{\mathrm{LJ}}(r) = 4\alpha\left[\left(\frac{\beta}{r}\right)^{12} - \left(\frac{\beta}{r}\right)^{6}\right], \tag{1}$$

where β, α, and r are the finite distance when the interparticle potential is zero, the potential depth, and the distance between atoms in two adjacent layers, respectively. Differentiating the above equation with respect to r results in the Lennard-Jones force function:

$$f_{\mathrm{LJ}}(r) = -\frac{dU_{\mathrm{LJ}}(r)}{dr} = 24\frac{\alpha}{\beta}\left[2\left(\frac{\beta}{r}\right)^{13} - \left(\frac{\beta}{r}\right)^{7}\right]. \tag{2}$$

The equivalent tensile-compressive modulus and shear modulus of the vdW layer are calculated calculating the strain

(change in $\boldsymbol{r}$) divided by the stress calculated as $\boldsymbol{F/A}$, where $F = \sum_A f_{\mathrm{LJ}}$ is the sum of the Lennard-Jones force of the atoms between the film and the substrate and $\boldsymbol{A}$ is the contact area between the film and the substrate. The details of the calculation are shown in Supplemental Material S1 [53]; the resulting tension and compression modulus are

$$E_v = h_v \sum_{i=1}^{N} \sum_{j=1}^{n} f_{ij}^{'}\left(r_{ij}^{zk}\right) \cos\theta_{ij}^{z}/A, \tag{3}$$

where f_{ij} represents the component of the vdW force between atom i in the upper layer and atom j in the lower layer at position k. $f_{ij}^{'}(r_{ij}^{zk})$ is the derivative of f_{ij} with respect to r. $\mathrm{h_v}$ represents the distance between the epilayer and the vdW substrate (i.e., vdW interfacial layer). θ_{ij}^{z} represents the angle between the line of the two atoms and the z axis, which is schematically shown in Fig. 1(c). N and n represent the total number of atoms in the upper and lower atomic layers, respectively, and r_{ij}^{zk} stands for the distance between two atoms moving in the z direction to position k. When moving to position k, the strain gradient between vdW layers is $\frac{\varepsilon_{zz}}{h_v}$, where $\varepsilon_{zz} = \frac{r_{ij}^{zk} - r_{ij}^{z0}}{h_v}$. Similarly, the shear modulus of the vdW interaction layer can be written as

$$G_v = h_v \sum_{i=1}^{N} \sum_{j=1}^{n} f_{ij}^{'}\left(r_{ij}^{xk}\right) \cos\theta_{ij}^{x} \sin\theta_{ij}^{z}/A, \tag{4}$$

where θ_{ij}^{x} represents the angle of the projection of the line in the lower layer between two atoms and the x axis, as shown in Fig. 1(c). When moving to position k, the shear strain gradient in the vdW interfacial layer is $\frac{\gamma_{xz}}{h_v}$, where $\gamma_{xz} = \frac{r_{ij}^{xk} - r_{ij}^{x0}}{h_v}$.

Next, we use this model to calculate the response of $BaTiO_3$ thin films grown on mica. We choose $BaTiO_3$ (BTO) because it is a well-known flexoelectric material whose flexoelectric coefficient in its bulk counterpart has been fully studied [14,58]. For the purpose of this work, BTO is also useful in that it is ferroelectric—and therefore piezoelectric—at room temperature, but it loses its ferroelectricity above T_c, so that temperature-dependent measurements allow discriminating between ferroelectricity and flexoelectricity—this will become important when comparing our theoretical calculations to experimental results. Meanwhile, muscovite mica was selected as an optimum vdW epitaxy substrate. Mica has a layered structure like that of graphite. Adjacent layers of mica are attracted by vdW force instead of chemical bonds, resulting in easy cleavage along the {001} planes. The cleaved surface is free of dangling bonds and has sixfold in-plane symmetry, which enables the growth of 111-oriented perovskite films [59,60].

We set the thickness of the vdW interfacial layer h_v to a finite distance β. We considered the case by setting the value of β to 0.166 nm, based on the interfacial bond distance extracted from transmission electron microscopy measurements of $SrTiO_3$ on mica [61,62]. In addition, it is obvious that the modulus has a linear relationship with the potential depth α. For the convenience of calculation, the potential depth for van der Waals bonds is assumed as a typical value $\alpha = 40$ meV, which is contained in the typical vdW bonding energy (40–70 meV) [51]. By combing Eq. (3) with Eq. (4), we get the relationship between the tensile-compressive, shear modulus and the strain gradient of the vdW interfacial layer, as shown in Fig. 1(d). Although the strain gradient of the vdW interfacial layer reaches an order of $10^5\ \mathrm{m^{-1}}$, the value of the shear modulus is still—three to four orders of magnitude lower than the tensile-compressive modulus. Therefore, when the sample is bent, the effects of the shear forces in plane can be ignored for the BTO epilayer meaning that the deformation of the substrate will not transfer in-plane strain onto the film. The film is only subjected to out-of-plane forces from the mica substrate, which ensures the film stays in contact with the substrate and thus tracks the bending of the substrates. Theoretically, then, the BTO films on mica substrate should be subjected only to strain gradient, without overall net strain of stretching or compression [Fig. 1(e)]. In contrast, both effects exist on the BTO film on STO substrate [Fig. 1(f)].

The deformation features of the films under pure bending can be further evidenced by finite element method (FEM) simulations, and compared with equivalent calculations for conventional epitaxy. The schematic diagrams and FEM calculations of the bending configuration for vdW and conventional epitaxy are shown in Fig. 2 and where the elastic constants of thin film BTO and single-crystal $SrTiO_3$ (STO) substrates are assumed. The used mechanical parameters of the substrate and epilayer can be found in Supplemental Material S2 [53]. The thickness of the BTO film is set to 100 nm and the thickness of the substrate is set to 1 μm which is ten times thicker than the film (this, of course, is still thinner than real substrates, but sufficient to illustrate the physics). the only difference between the two calculations is the interfacial bond. In order to simulate the vdW interaction between the film and the mica substrate, a thin elastic plate (1 nm) is inserted at the interface, represented by a purple line in Fig. 2(a) (see Supplemental Material S3 [53]). The elastic and shear modulus of the thin elastic plate are set to 60 GPa and 2 MPa respectively, which correspond to the values obtained in Fig. 1(d). Three-point bending is achieved by applying linearly distributed normal stress in the lower left end and lower right of the substrate. In order to approach the strain gradient level in our experiments, the bending moment is set to $1.0417e^{-10}$ N m (the strain gradient of the substrate is $\sim 0.05\ \mathrm{m^{-1}}$).

The strain ε_{11} distribution of the mica-based BTO film is shown in Fig. 2(b). The strain discontinuity along the thickness direction in the BTO/mica system can be clearly seen. The dotted line is used to mark the part of $\varepsilon_{11} = 0$, where a neutral plane occurs. The results show that there are two neutral planes in the BTO/mica system, with one located at the center of the mica while the other is inside the BTO film itself. The bending state of the BTO/STO heterostructure is also simulated. The elastic and shear modulus of the interfacial elastic plate in this case are same as that of BTO. Under the same bending moment, the strain ε_{11} distribution of the STO-based BTO film is obtained as shown in Fig. 2(d). Since the shear modulus cannot be neglected here, the strain imposed by the substrate carries across the interfacial layer and varies continuously across the film-substrate system. Only one neutral plane exists, which is located near the center of the STO substrate.

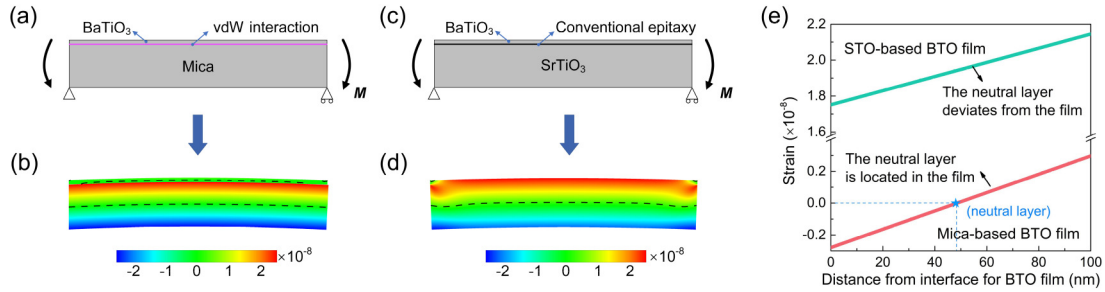

FIG. 2. Schematic illustration of the FEM model of mica-based and $SrTiO_3$-based $BaTiO_3$ thin films, and the strain ε_{11} results of the $BaTiO_3$ films under the condition of bending moment. (a) The bending model of mica-based $BaTiO_3$ thin film, (b) the strain ε_{11} of the substrate and the film along the thickness direction show discontinuity. (c) The bending model of $SrTiO_3$-based $BaTiO_3$ thin film, (d) the strain ε_{11} of the substrate and the film along the thickness direction show continuity. (e) The strain ε_{11} distribution of 100-nm thin $BaTiO_3$ films along the thickness direction. For mica-based $BaTiO_3$ thin film, the neutral layer of $BaTiO_3$ thin film is located in the film (the shear modulus is still there, which make the neutral layer not in the center of the thickness. However, the ratio of offset to thickness is only 1.5%), so that there is compressive strain on one side and tensile on the other, and the average strain is therefore close to it. Conversely, the neutral layer of $BaTiO_3$ thin film attached to $SrTiO_3$ by conventional epitaxy is outside of the film (it coincides with the substrate's neutral plane) and thus there is a net strain on the film when the substrate is bent.

The strain ε_{11} distribution of BTO thin films grown on these two substrates along the thickness direction is summarized in Fig. 2(e). For the mica-based epilayer, since the neutral plane (which, by definition, is where the in-plane strain is zero) lies close to the center of the film, the net strain on the BTO layer is negligible, and the polarization of the mica-based BTO epilayer will mainly come from the strain gradient. Conversely, for the epitaxial system, there is only one neutral plane and it is deep inside the substrate. As a consequence, the BTO epilayer displays a large net tensile strain as there is no neutral plane inside the film. The polarization caused by this tensile strain will generate piezoelectric polarization in the BTO/STO heterostructure. For this reason, measurements of the flexoelectric coefficient of conventional epitaxial films using the standard setup of bulk materials will be contaminated or even dominated by piezoelectricity.

To validate experimentally our predictions, we have grown thin film heterostructures on vdW substrates (mica) and oxide substrates (STO) respectively, and compared their properties. The thin film capacitor heterostructures of $SrRuO_3$/BTO/$SrRuO_3$ were deposited in both cases by pulsed laser deposition (see Fig. S2 in Supplemental Material S4 [53]), with the 50-nm-thick $SrRuO_3$ (SRO) layers acting as electrodes.

III. STRUCTURAL CHARACTERIZATION OF THIN FILMS ON MICA AND STO SUBSTRATES

Figure 3(a) shows typical out-of-plane $2\theta/\omega$ scans of the BTO/SRO/STO and BTO/SRO/mica heterostructures. The observation of only BTO (lll) and SRO (lll) diffraction peaks on STO (lll) and mica ($00l$) substrates discloses the highly coherent orientation of the BTO/SRO thin films and the absence of detectable cristalline impurities [46,63]. The BTO (222) and SRO (222) peak positions of the films grown on mica are close to the hypothetical bulk BTO and SRO values, suggesting that these films are fully relaxed. In contrast, for the films grown on STO the out-of-plane lattice parameter is larger than the bulk value. The epitaxial relationships and strain state can be better assessed by off-specular reciprocal space maps, which allow simultaneous access to in-plane and out-of-plane lattice parameters. These are shown in Fig. 3(c). It can be seen that, for heterostructures grown on STO, the SRO is in-plane coherent with the substrate while the BTO is partially relaxed. In contrast, for the heterostructures grown on mica, the BTO is fully coherent with the SRO electrode. It can furthermore be seen that the in-plane reciprocal distance of the STO-grown BTO film is slightly smaller, and therefore the lattice parameter is larger than that of the STO-grown one. Given that the out-of-plane lattice parameter of the films on STO was also larger than in bulk, we conclude that the films grown on STO have a larger unit-cell volume than those grown on mica (see Supplemental Material S5 [53]). An expanded unit cell is often a tell-tale sign of oxygen vacancies in the perovskite structure [64].

The conclusions from the crystallographic analysis are therefore that (i) in the mica-grown heterostructures, the ferroelectric layer is in-plane coherent with the electrode, but the entire capacitor is fully relaxed from the substrate, as indicated by the off-specular RSM and bulklike value of the lattice parameters and (ii) in the STO-grown capacitors, the electrode is fully coherent with the substrate while the ferroelectric layer is partially relaxed and also shows an expanded lattice suggestive of increased oxygen vacancies. We now turn our attention to the functional response.

IV. DIELECTRIC AND FERROELECTRIC CHARACTERISTICS OF THIN FILMS ON MICA AND STO SUBSTRATES

The dielectric constant and loss as a function of temperature [Fig. 4(a)] shows that the BTO capacitors grown on mica have a critical temperature very close to that of bulk BTO ($T_c \sim 150\,^{\circ}$C vs $130\,^{\circ}$C in bulk), with a sharp, first-order peak at the Curie temperature. The proximity of the film's Curie temperature to bulk is consistent with the absence of epitaxial strain, with the relatively small upward shift probably being due to the small compressive strain induced by the SRO

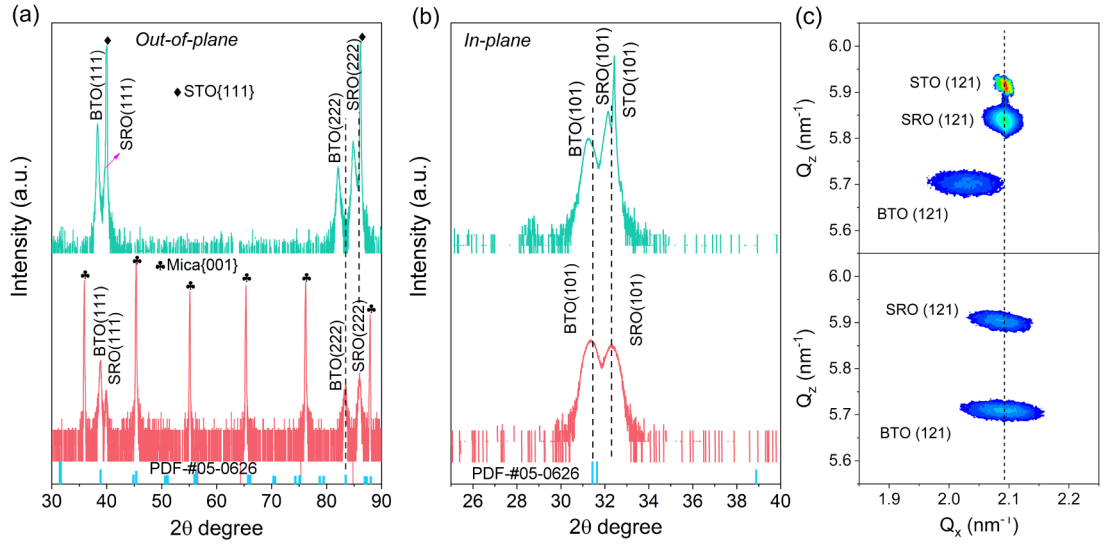

FIG. 3. Typical XRD out-of-plane (a) and in-plane (b) $2\theta/\omega$ scan image for the BTO/SRO/STO (green) and BTO/SRO/STO/mica (red) heterostructures. (c) The in-plane RSMs taken around the BTO (121) peaks for STO-based and mica-based heterostructures.

electrodes. Likewise, the first-order nature of the transition is also fully consistent with the absence of in-plane clamping in these structures [65]. In contrast, the STO-grown films have no dielectric anomaly within our measured temperature range, suggesting that their residual epitaxial strain is sufficient to push $T_c$above the highest measured temperature of 240 °C [66,67]. Their losses were also higher, consistent with the suspected presence of oxyen vacancies. The room temperature dielectric constant and loss as a function of frequency for mica-based BTO film and STO-based BTO film can be seen in Fig. S4 of Supplemental Material S6 [53].

In addition, room temperature ferroelectricity was probed by means of piezoresponse force microscopy (PFM) hysteresis loops, as shown in Figs. 4(b) and 4(c). The amplitude and phase images of BTO films on STO and mica substrates can be seen in Fig. S5 of Supplemental Material S7 [53]. The square hysteresis loops with 180° phase difference are consistent with the presence of robust ferroelectricity in both films. There is, however, a telling difference in imprint: while the conventional-epitaxy system shows strong imprint (the hysteresis loops is off-centered by −3 V), the vdW heterostructure shows virtually no imprint, with the hysteresis loop centered at 0 V. Given that the top and bottom electrodes are identical in both capacitors, the source of imprint cannot be attributed to a chemical or interfacial field difference. Instead, the results are consistent with a difference in the flexoelectric built-in field, which is 0 for the vdW structure (the strain is fully relaxed) and nonzero in the epitaxial capacitor due to the partial strain relaxation. The *P-E* loops of BTO films on STO and mica substrates can be seen in Fig. S6 of Supplemental Material S8 [53].

V. RESULTS AND DISCUSSION

The flexoelectric coefficients of the thin films were then measured using a dynamic mechanical analyzer (DMA, DMA 850, TA Instruments, USA) system (see Supplemental Material S9 [53]). To determine whether or not there is a piezoelectric contribution to the bending-induced polarization, a set of samples with different substrate thicknesses were investigated (Fig. 5) (sets with different film thickness were also measured and shown in Fig. S8 in Supplemental Material S10 [53]); the idea is that, whereas bending-induced strain gradient (and therefore flexoelectricity) depends only

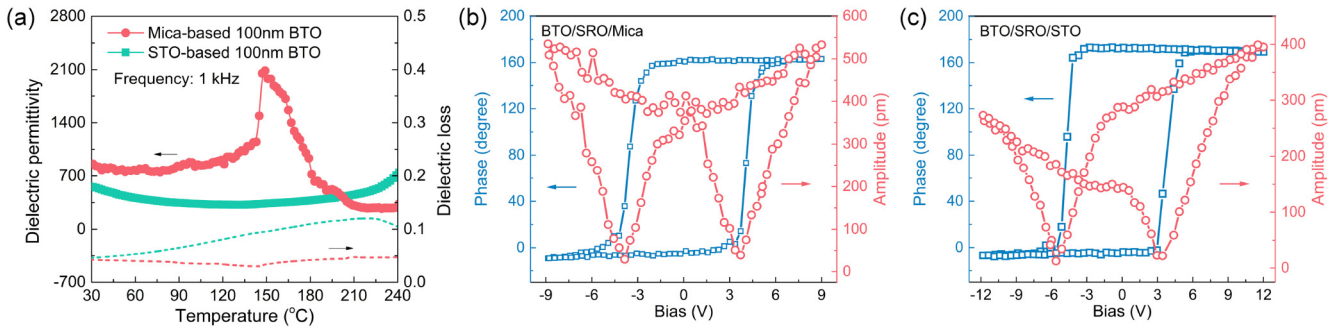

FIG. 4. (a) Temperature dependence of dielectric properties of 100-nm BTO films on mica substrate and STO substrate. (b), (c) Piezoresponse force microscopy loops for films grown respectively on STO (conventional epitaxy) and mica (vdW epitaxy).

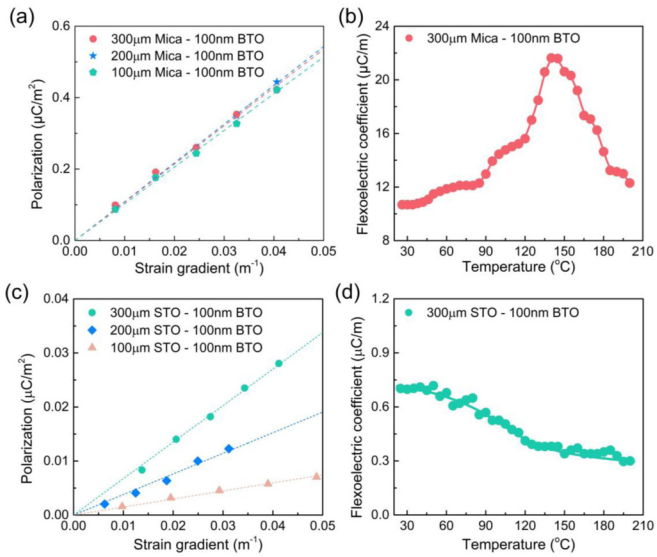

FIG. 5. (a) Flexoelectric polarization as a function of strain gradient in various mica-based BTO thin films with different thicknesses of mica substrate. (b) Temperature dependence of flexoelectric coefficients of the 300-μm mica, 100-nm BTO thin films. (c) Flexoelectric polarization as a function of strain gradient in various STO-based BTO thin films with different thicknesses of STO substrate. (d) Temperature dependence of flexoelectric coefficients of the 300-μm STO, 100-nm BTO thin films.

on curvature and is independent of the total thickness of the system, bending-induced interfacial strain (and therefore piezoelectricity) is directly proportional to substrate thickness. Real flexoelectricity will therefore show up as a thickness-independent flexoelectric coefficient, whereas bending-induced piezoelectricity will show up as a proportionality between the apparent flexoelectric coefficient and the substrate thickness. For mica-based BTO thin films [Fig. 5(a)], we see that all the samples have almost identical flexoelectric coefficients (nearly 10 μC/m), irrespective of the substrate thickness, consistent with intrinsic flexoelectricity and in agreement with the expectation for the vdW model (see Supplemental Material S11 [53]). Moreover, the actual value of the flexoelectric coefficient is similar to that reported for bulk [14,58,68], and the temperature dependence of the flexoelectric coefficient of mica-based BTO thin film [Fig. 5(b)] tracks the bulklike dielectric constant of the film [Fig. 4(a)]. These results are therefore fully consistent with the hypothesis that vdW epitaxy effectively removes substrate influence from the flexoelectric response of the films.

In addition, it is worth emphasizing that mica has a multilayer structure connected by vdW forces, just like the BTO film grown on the mica substrate, and may have finite slippage between the layers. What we can therefore say is that (i) in the experiments, it is likely that at least some of the curvature-induced strain will be relaxed inside the substrate, rather than the substrate-film interface, but (ii) even if we neglect completely this internal relaxation (as we did in our model), the calculations indicate that the substrate-film interface alone is capable of relaxing the strain.

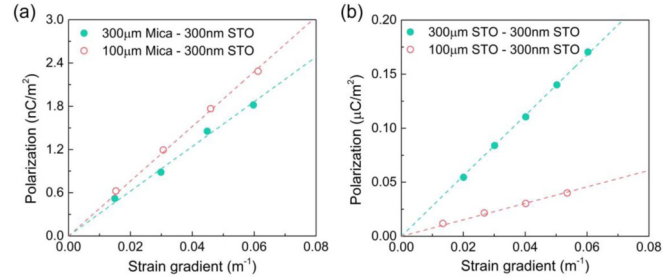

FIG. 6. (a) Flexoelectric polarization as a function of strain gradient in various mica-based STO thin films with different thicknesses of mica substrate. (b) Flexoelectric polarization as a function of strain gradient in various STO-based STO thin films with different thicknesses of STO substrate.

In contrast, for the STO-based BTO thin films, changing the thickness of STO substrate causes a proportional change in the bending-induced polarization [Fig. 5(c)]. This proves that the measured polarization is not all of flexoelectric origin and must also have a piezoelectric component, piezoelectricity being proportional to bending-induced strain, which in turn is proportional to substrate thickness. The effective flexoelectric coefficients (polarization divided by curvature) are smaller those of bulk BTO, suggesting that piezoelectric and flexoelectric polarizations have opposite signs and partially cancel each other (see Supplemental Material S12 [53]) (piezoelectric modulation of flexoelectricity in this kind of capacitors has been observed before, Ref. [69]). The temperature dependence of the effective flexoelectric coefficient, shown in Fig. 4(d), shows no peak at around the Curie temperature of BTO and instead increases as temperature is decreased. This is also consistent with a dominant role of piezoelectricity, which is proportional to the ferroelectric polarization and therefore grows with decreasing temperature.

Finally, to expand the generality of our results, we measured also the flexoelectricity of STO thin films, bulk STO being a cubic perovskite that, not being piezoelectric in bulk, is regarded as a good archetype for flexoelectric research [15]. Figure 6 presents the flexoelectric polarization of STO thin films with different substrate thicknesses as a function of strain gradient. The flexoelectricity of samples with constant substrate thickness but different film thicknesses is shown in Figs. S8c and S8d [53]. The vdW (mica-grown) heterostructures demonstrate a flexoelectric coefficient of about 30 nC/m with only a weak thickness dependence. This is larger than, but still comparable to, the flexoelectric coefficient of bulk STO, which is around 5 nC/m [15]. In contrast, the STO/SRO/STO_{sub} epitaxial heterostructures display a much larger and thickness-dependent effective flexoelectric coefficient: for the STO substrate with a thickness of 300 μm, the flexoelectric coefficient is 2.8 μC/m, but when the substrate thickness reduces to 100 μm, the flexoelectric coefficient decreases to 0.7 μC/m. Both the enormous enhancement with respect to the bulk value and the proportionality to substrate thickness are consistent with a dominant role of piezoelectricity for the conventional epitaxy films. Here it is also worth pointing out that,

although cubic $SrTiO_3$ should not be piezoelectric, residual piezoelectricity can exist even in bulk [15], and homoepitaxial thin films do show relaxor ferroelectricity at room temperature [70].

The aforementioned results indicate that the functional properties in general, and in particular the flexoelectric response of vdW epilayers, are not strongly affected by the substrate, and are moreover surprisingly similar to those of the bulk compounds, despite the difference in thickness between our thin films and bulk single crystals. Under bending, vdW epilayers retain their own neutral plane (see Fig. 2 and Fig. S7 [53]) and respond like a bulk material. In contrast, for traditional epitaxy, the loss of neutral plane in the film induced by the strong interface interaction introduces an additional contribution from strain. This generates a piezoelectric component in the bending-induced polarization that masks the true flexoelectricity of the films.

The present work shows that mica-based vdW epitaxy is a powerful tool for measuring the intrinsic properties of thin films and their response to bending.

ACKNOWLEDGMENTS

This work was supported by the National Natural Science Foundation of China (Grants No. 12174174, No. 51962020, No. 51972157, No. 51702149, No. 11604135, and No. 11964017) and the Natural Science Foundation of Jiangxi Province (Grants No. 20212ACB214011, No. 20202ZDB01006, and No. 20192ACB21017) were also acknowledged. G.C. also acknowledges financial support from Project No. PID2019-108573GB-C21 funded by MCIN/AEI/10.13039/501100011033 and Severo Ochoa Grant No. SEV-2017-0706. L.S. thanks for support from Nanchang University.

[1] A. Abdollahi, F. Vasquez-Sancho, and G. Catalan, Piezoelectric Mimicry of Flexoelectricity, Phys. Rev. Lett. **121**, 205502 (2018).

[2] R. Guo, L. You, W. Lin, A. Abdelsamie, X. Shu, G. Zhou, S. Chen, L. Liu, X. Yan, J. Wang, and J. Chen, Continuously controllable photoconductance in freestanding $BiFeO_3$ by the macroscopic flexoelectric effect, Nat. Commun. **11**, 2571 (2020).

[3] L. Shu, X. Wei, T. Pang, X. Yao, and C. Wang, Symmetry of flexoelectric coefficients in crystalline medium, J. Appl. Phys. **110**, 104106 (2011).

[4] M. Stengel, Microscopic response to inhomogeneous deformations in curvilinear coordinates, Nat. Commun. **4**, 2693 (2013).

[5] G. Catalan, A. Lubk, A. H. G. Vlooswijk, E. Snoeck, C. Magen, A. Janssens, G. Rispens, G. Rijnders, D. H. A. Blank, and B. Noheda, Flexoelectric rotation of polarization in ferroelectric thin films, Nat. Mater. **10**, 963 (2011).

[6] K. Chu, B. Jang, J. Sung, Y. Shin, E. Lee, K. Song, J. Lee, C. Woo, S. Kim, S. Choi, and T. Koo, Enhancement of the anisotropic photocurrent in ferroelectric oxides by strain gradients, Nat. Nanotechnol. **10**, 972 (2015).

[7] J. Narvaez and G. Catalan, Origin of the enhanced flexoelectricity of relaxor ferroelectrics, Appl. Phys. Lett. **104**, 162903 (2014).

[8] X. Wen, D. Li, K. Tan, Q. Deng, and S. Shen, Flexoelectret: An Electret with a Tunable Flexoelectriclike Response, Phys. Rev. Lett. **122**, 148001 (2019).

[9] S. Park, B. Wang, T. Paudel, S. Park, S. Das, J. Kim, E. Ko, H. Lee, N. Park, L. Tao, D. Suh, E. Tsymbal, L. Chen, T. Noh, and D. Lee, Colossal flexoresistance in dielectrics, Nat. Commun. **11**, 2586 (2020).

[10] M. Stengel, Flexoelectricity from density-functional perturbation theory, Phys. Rev. B **88**, 174106 (2013).

[11] A. Kvasov and A. K. Tagantsev, Dynamic flexoelectric effect in perovskites from first principles calculations, Phys. Rev. B **92**, 054104 (2015).

[12] J. Hong and D. Vanderbilt, First-Principles theory and calculation of flexoelectricity, Phys. Rev. B **88**, 174107 (2013).

[13] A. Biancoli, C. Fancher, J. Jones, and D. Damjanovic, Breaking of macroscopic centric symmetry in paraelectric phases of ferroelectric materials and implications to flexoelectricity, Nat. Mater. **14**, 224 (2015).

[14] J. Narvaez, S. Saremi, J. Hong, M. Stengel, and G. Catalan, Large Flexoelectric Anisotropy in Paraelectric Barium Titanate, Phys. Rev. Lett. **115**, 037601 (2015).

[15] P. Zubko, G. Catalan, A. Buckley, P. Welche, and J. Scott, Strain-Gradient-Induced Polarization in $SrTiO_3$ Single Crystals, Phys. Rev. Lett. **99**, 167601 (2007).

[16] O. Lavrentovich, V. Nazarenko, V. Sergan, and G. Durand, Dielectric quenching of the electric polar surface instability in a nematic liquid crystal, Phys. Rev. A **45**, R6969 (1992).

[17] M. Ravnik and J. C. Everts, Topological-Defect Induced Surface-Charge Heterogeneities in Nematic Electrolytes, Phys. Rev. Lett. **125**, 037801 (2020).

[18] Q. Deng, L. Liu, and P. Sharma, Electrets in soft Materials: Nonlinearity, size Effects, and giant electromechanical coupling, Phys. Rev. E **90**, 012603 (2014).

[19] F. Vasquez-Sancho, A. Abdollahi, D. Damjanovic, and G. Catalan, Flexoelectricity in bones, Adv. Mater. **30**, 1705316 (2018).

[20] P. Zhang, A. Keleshian, and F. Sachs, Voltage-Induced membrane movement, Nature (London) **413**, 428 (2001).

[21] F. Ahmadpoor and P. Sharma, Flexoelectricity in two-dimensional crystalline and biological membranes, Nanoscale **7**, 16555 (2015).

[22] J. Narvaez, F. Sancho, and G. Catalan, Enhanced flexoelectric-like response in oxide semiconductors, Nature (London) **538**, 219 (2016).

[23] L. Shu, S. Ke, L. Fei, W. Huang, Z. Wang, J. Gong, X. Jiang, L. Wang, F. Li, S. Lei, Z. Rao, Y. Zhou, R. Zheng, X. Yao, Y. Wang, M. Stengel, and G. Catalan, Photoflexoelectric effect in halide perovskites, Nat. Mater. **19**, 605 (2020).

[24] L. Wang, S. Liu, X. Feng, C. Zhang, L. Zhu, J. Zhai, Y. Qin, and Z. Wang, Flexoelectronics of centrosymmetric semiconductors, Nat. Nanotechnol. **15**, 661 (2020).

[25] A. Zabalo and M. Stengel, Switching a Polar Metal Via Strain Gradients, Phys. Rev. Lett. **126**, 127601 (2021).

[26] M. S. Majdoub, P. Sharma, and T. Cagin, Enhanced size-dependent piezoelectricity and elasticity in nanostructures due to the flexoelectric effect, Phys. Rev. B **77**, 125424 (2008).
[27] T. Nguyen, S. Mao, W. Yao, P. Purohit, and M. Mcalpine, Nanoscale flexoelectricity, Adv. Mater. **25**, 946 (2013).
[28] U. Bhaskar, N. Banerjee, A. Abdollahi, Z. Wang, D. Schlom, G. Rijnders, and G. Catalan, A flexoelectric microelectromechanical system on silicon, Nat. Nanotechnol. **11**, 263 (2016).
[29] B. Wang, H. Lu, C. Bark, C. Eom, A. Gruverman, and L. Chen, Mechanically induced ferroelectric switching in BaTiO3 thin films, Acta. Mater. **193**, 151 (2020).
[30] H. Lu, C. Bark, D. Ojos, J. Alcala, C. Eom, G. Catalan, and A. Gruverman, Mechanical writing of ferroelectric polarization, Science **336**, 59 (2012).
[31] S. Park, B. Wang, S. Das, S. Chae, J. Chung, J. Yoon, L. Chen, S. Yang, and T. Noh, Selective control of multiple ferroelectric switching pathways using a trailing flexoelectric field, Nat. Nanotechnol. **13**, 366 (2018).
[32] F. Zhang, P. Lv, Y. Zhang, S. Huang, C. Wong, H. Yau, X. Chen, Z. Wen, X. Jiang, C. Zeng, J. Hong, and J. Dai, Modulating the Electrical Transport in the Two-Dimensional Electron Gas at $LaAlO_3/SrTiO_3$ Heterostructures by Interfacial Flexoelectricity, Phys. Rev. Lett. **122**, 257601 (2019).
[33] M. Yang, D. Kim, and M. Alexe, Flexo-Photovoltaic effect, Science **360**, 904 (2018).
[34] K. Cordero-Edwards, H. Kianirad, C. Canalias, J. Sort, and G. Catalan, Flexoelectric Fracture-Filter Effect in Ferroelectrics, Phys. Rev. Lett. **122**, 135502 (2019).
[35] X. Yu, L. Wu, B. Zhang, H. Zhou, and M. Gan, Thickness-Dependent polarization-induced intrinsic magnetoelectric effects in $La_{0.67}Sr_{0.33}MnO_3/PbZr_{0.52}Ti_{0.48}O_3$ heterostructures, Phys. Rev. B **100**, 104405 (2019).
[36] C. Tan, J. Chen, X. Wu, and H. Zhang, Epitaxial growth of hybrid nanostructures, Nat. Rev. Mater. **3**, 17089 (2018).
[37] B. Lalmi, H. Oughaddou, H. Enriquez, A. Kara, S. Vizzini, B. Ealet, and B. Aufray, Epitaxial growth of a silicene sheet, Appl. Phys. Lett. **97**, 223109 (2010).
[38] M. Tyunina, J. Narkilahti, M. Plekh, R. Oja, R. Nieminen, A. Dejneka, and V. Trepakov, Evidence for Strain-Induced Ferroelectric Order in Epitaxial Thin-Film $KTaO_3$, Phys. Rev. Lett. **104**, 227601 (2010).
[39] J. Ouyang and A. Roytburd, Intrinsic effective piezoelectric coefficients of an epitaxial ferroelectric film, Acta Mater. **54**, 531 (2006).
[40] J. Očenášek, H. Lu, C. W. Bark, C. B. Eom, J. Alcalá, G. Catalan, and A. Gruverman, Nanomechanics of flexoelectric switching, Phys. Rev. B **92**, 035417 (2015).
[41] G. Dong, S. Li, M. Yao, Z. Zhou, Y. Zhang, X. Han, Z. Luo, J. Yao, B. Peng, Z. Hu, H. Huang, T. Jia, J. Li, W. Ren, Z. Ye, X. Ding, J. Sun, C. W. Nan, L. Chen, J. Li, and M. Liu, Super-Elastic ferroelectric single-crystal membrane with continuous electric dipole rotation, Science **366**, 475 (2019).
[42] M. Herman and H. Sitter, *Molecular Beam Epitaxy* (Springer, Berlin, 1996).
[43] R. Guzman, L. Maurel, E. Langenberg, A. Lupini, P. Algarabel, J. Pardo, and C. Magen, Polar-Graded multiferroic $SrMnO_3$ thin films, Nano Lett. **16**, 2221 (2016).
[44] A. Koma, K. Sunouchi, and T. Miyajima, Fabrication and characterization of heterostructures with subnanometer thickness, Microelectron. Eng. **2**, 129 (1984).
[45] A. Koma, Van der waals Epitaxy-a new epitaxial growth method for a highly lattice-mismatched system, Thin Solid Films **216**, 72 (1992).
[46] L. Dai, G. Niu, J. Zhao, H. Zhao, Y. Liu, Y. Wang, Y. Zhang, H. Wu, L. Wang, D. Pfutzenreuter, J. Schwarzkopf, C. Dubourdieu, T. Schroeder, Z. Ye, Y. Xie, and W. Ren, Toward van der Waals epitaxy of transferable ferroelectric barium titanate films via a graphene monolayer, J. Mater. Chem. C **8**, 3445 (2020).
[47] J. Wu, Z. Liang, C. Ma, G. Hu, L. Shen, Z. Sun, Y. Zhang, L. Lu, M. Liu, and C. Jia, Flexible lead-free $BaTiO_3$ ferroelectric elements with high performance, IEEE Electron Device Lett. **40**, 889 (2019).
[48] R. Jia, H. Kum, X. Sun, Y. Guo, B. Wang, P. Fang, J. Jiang, D. Gall, T. Lu, M. Washington, J. Kim, and J. Shi, Van der waals epitaxy and remote epitaxy of $LiNbO_3$ thin films by pulsed laser deposition, J. Vac. Sci. Technol. A **39**, 040405 (2021).
[49] Y. Wang, Y. Shi, G. Xin, J. Lian, and J. Shi, Two-Dimensional van der waals epitaxy kinetics in a three-dimensional perovskite halide, Cryst. Growth Des. **15**, 4741 (2015).
[50] Y. Wang, L. Gao, Y. Yang, Y. Xiang, Z. Chen, Y. Dong, H. Zhou, Z. Cai, G.-C. Wang, and J. Shi, Nontrivial strength of van der Waals epitaxial interaction in soft perovskites, Phys. Rev. Materials **2**, 076002 (2018).
[51] S. Butler, S. Hollen, L. Cao, Y. Cui, J. Gupta, H. Gutierrez, T. Heinz, S. Hong, J. Huang, A. Ismach, E. Johnston-Halperin, M. Kuno, V. Plashnitsa, R. Robinson, R. Ruoff, S. Salahuddin, J. Shan, L. Shi, M. Spencer, M. Terrones, W. Windl, and J. Goldberger, Opportunities in two-dimensional materials beyond graphene, ACS Nano **7**, 2898 (2013).
[52] M. I. Baskes, Many-Body Effects in Fcc Metals: A Lennard-Jones Embedded-Atom Potential, Phys. Rev. Lett. **83**, 2592 (1999).
[53] See Supplemental Material at http://link.aps.org/supplemental/10.1103/PhysRevB.106.024108 for (1) a detailed calculation method to simulate the vdW interaction; (2) sample information; (3) strain state of BTO films; (4) ferroelectric, dielectric, and flexoelectric properties of BTO films on STO and mica substrates, which includes Refs. [22,54–57,64,70].
[54] K. Choi, M. Biegalski, Y. Li, A. Sharan, J. Schubert, R. Uecker, P. Reiche, Y. Chen, X. Pan, V. Gopalan, L. Chen, D. Schlom, and C. Eom, Enhancement of ferroelectricity in strained BaTiO3 thin films, Science **306**, 1005 (2004).
[55] E. Weisstien, "Curvature," Wolfram Mathworld, retrieved 19 June 2022.
[56] W. James, R. Newnham, and G. Gibbs, Grystal structure analysis of synthetic fluorophlogopite, Am. Mineral. **58**, 249 (1973).
[57] H. Christenson and N. Thomson, The nature of the air-cleaved mica surface, Surf. Sci. Rep. **71**, 367 (2016).
[58] W. Ma and L. Cross, Flexoelectricity of barium titanate, Appl. Phys. Lett. **88**, 232902 (2006).
[59] S. Ke, J. Xie, C. Chen, P. Lin, X. Zeng, L. Shu, L. Fei, Y. Wang, M. Ye, and D. Wang, Van der waals epitaxy of al-doped ZnO film on mica as a flexible transparent hheater with ultrafast thermal response, Appl. Phys. Lett. **112**, 031905 (2018).
[60] Y. Bitla and Y. Chu, MICAtronics: A new platform for flexible x-tronics, FlatChem **3**, 26 (2017).
[61] L. Lu, Y. Dai, H. Du, M. Liu, J. Wu, Y. Zhang, Z. Liang, S. Raza, D. Wang, and C. Jia, Atomic scale understanding of

the epitaxy of perovskite oxides on flexible mica substrate, Adv. Mater. Interfaces **7**, 1901265 (2019).

[62] H. Liu, C. Wang, D. Su, T. Amrillah, Y. Hsieh, K. Wu, Y. Chen, J. Juang, L. Eng, S. Jen, and Y. Chu, Flexible heteroepitaxy of $CoFe_2O_4$/Muscovite bimorph with large magnetostriction, ACS Appl. Mater. Interfaces **9**, 7297 (2017).

[63] A. Chen, F. Khatkhatay, W. Zhang, C. Jacob, L. Jiao, and H. Wang, Strong oxygen pressure dependence of ferroelectricity in $BaTiO_3/SrRuO_3/SrTiO_3$ epitaxial heterostructures, J. Appl. Phys. **114**, 124101 (2013).

[64] H. Ullmann and N. Trofimenko, Estimation of effective ionic radii in highly defective perovskite-type oxides from experimental data, J. Alloy. Compd. **316**, 153 (2001).

[65] N. A. Pertsev, A. G. Zembilgotov, and A. K. Tagantsev, Effect of Mechanical Boundary Conditions on Phase Diagrams of Epitaxial Ferroelectric Thin Films, Phys. Rev. Lett. **80**, 1988 (1998).

[66] F. Bai, H. Zheng, H. Cao, L. Cross, R. Ramesh, J. Li, and D. Vieland, Epitaxially induced high temperature (>900 K) cubic-tetragonal structural phase transition in $BaTiO_3$ thin films, Appl. Phys. Lett. **85**, 4109 (2004).

[67] N. A. Pertsev and V. G. Koukhar, Polarization Instability in Polydomain Ferroelectric Epitaxial Thin Films and the Formation of Heterophase Structures, Phys. Rev. Lett. **84**, 3722 (2000).

[68] T. Hu, Q. Deng, X. Liang, and S. Shen, Measuring the flexoelectric coefficient of bulk barium titanate from a shock wave experiment, J. Appl. Phys. **122**, 055106 (2017).

[69] H. Wu, S. Lu, T. Aoki, P. Ponath, J. Wang, C. Young, J. Ekerdt, M. McCartney, and D. Smith, Direct observation of large atomic polar displacements in epitaxial barium titanate thin films, Adv. Mater. Interfaces **7**, 2000555 (2020).

[70] H. Jang, A. Kumar, S. Denev, M. Biegalski, P. Maksymovych, C. Bark, C. Nelson, C. Folkman, S. Baek, N. Balke, C. Brooks, D. Tenne, D. Schlom, L. Chen, X. Pan, S. Kalinin, V. Gopalan, and C. Eom, Ferroelectricity in Strain-Free $SrTiO_3$ Thin Films, Phys. Rev. Lett. **104**. 197601 (2010).